

# Measurement of global spin alignment of vector mesons at RHIC\*

SUBHASH SINGHA (FOR STAR COLLABORATION)

Institute of Modern Physics Chinese Academy of Sciences, Lanzhou, China 73000  
(subhash@impcas.ac.cn)

*Received July 29, 2022*

1 We report the measurements of spin alignment ( $\rho_{00}$ ) for  $K^{*0}$ ,  $\overline{K^{*0}}$ ,  $K^{*+}$ ,  
2 and  $K^{*-}$  vector mesons in RHIC isobar collisions (Zr+Zr and Ru+Ru) at  
3  $\sqrt{s_{\text{NN}}} = 200$  GeV. We observe the first non-zero spin alignment for  $K^{*\pm}$  in  
4 heavy-ion collisions. The  $K^{*\pm}$   $\rho_{00}$  is about  $3.9\sigma$  larger than that of  $K^{*0}$ .  
5 The observed difference and the ordering between  $K^{*\pm}$  and  $K^{*0}$  are sur-  
6 prising, and require further inputs from theory. When comparing between  
7 the isobar and Au+Au collisions, no significant system size dependence in  
8  $K^{*0}$   $\rho_{00}$  is observed within uncertainties.

## 9 1. Introduction

10 In the initial stage of a non-central heavy-ion collisions (HIC), a large  
11 orbital angular momentum (OAM) is imparted into the system. The mag-  
12 nitude of such OAM can be  $\sim bA\sqrt{s_{\text{NN}}} \sim 10^4\hbar$ , where  $b$  is the impact  
13 parameter and  $A$  is the mass number of the collision species [1]. A part of  
14 OAM transferred to the Quark Gluon Plasma (QGP) medium can polarize  
15 quarks and anti-quarks due to “spin-orbit” interaction and hence induce a  
16 non-vanishing polarization for hadrons with non-zero spin [2]. The incoming  
17 charged spectators in HIC can also induce a large but short lived electro-  
18 magnetic field ( $eB \sim 10^{18}$  Gauss) [3]. Such a strong  $B$ -field can also polarize  
19 both quarks and anti-quarks due to its coupling with the intrinsic magnetic  
20 moment. The measurement of spin polarization can not only offer insights  
21 into the initial orbital angular momentum interactions and magnetic field,  
22 but also serve as an experimental probe to understand the response of QGP  
23 medium under these extreme initial conditions. The measurement of sig-  
24 nificant non-zero polarization of  $\Lambda$  hyperons by STAR collaboration offered

---

\* Presented at the 29<sup>th</sup> International Conference on Ultra-relativistic Nucleus-Nucleus Collisions (Quark Matter 2022), Krakow, Poland. SS is supported by the Strategic Priority Research Program of Chinese Academy of Sciences.

25 first experimental evidence of the presence of vorticity of the QGP medium  
 26 induced by the initial angular momentum, while a hint of difference between  
 27  $\Lambda$  and  $\bar{\Lambda}$  spin polarization at RHIC presents an opportunity to probe the  
 28 initial  $B$  field [4]. The spin alignment is quantified by 00<sup>th</sup> element of the  
 29 spin density matrix,  $\rho_{00}$ , and can be measured from the angular distribution  
 30 of the decay daughter of the vector meson [5]:

$$\frac{dN}{d\cos\theta^*} \propto \left( (1 - \rho_{00}) + (3\rho_{00} - 1)\cos^2\theta^* \right), \quad (1)$$

31 where  $\theta^*$  is the angle between the polarization axis and momentum direction  
 32 of the daughter particle in the rest frame of its parent. For global spin  
 33 alignment, the polarization axis is chosen as the direction perpendicular to  
 34 the reaction plane, which can be correlated with both the OAM and the  
 35  $B$ -field. The value of  $\rho_{00}$  is expected to be  $\frac{1}{3}$  in absence of spin alignment,  
 36 while a deviation of  $\rho_{00}$  from  $\frac{1}{3}$  indicates a net spin alignment.

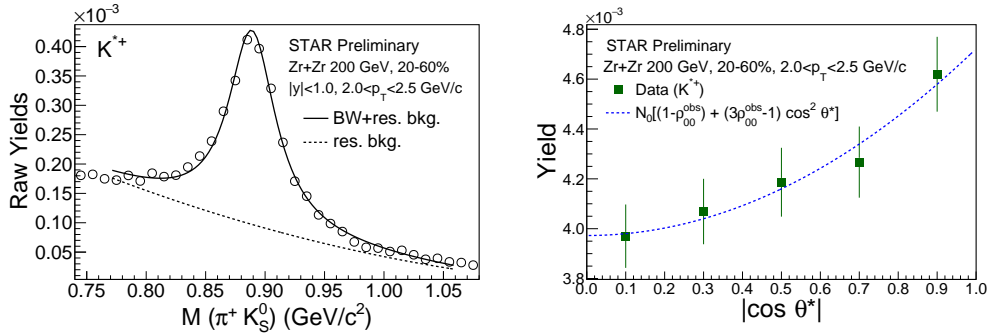


Fig. 1. Left:  $K^{*+}(\rightarrow \pi^+ + K_S^0)$  invariant mass distribution for  $2.0 < p_T < 2.5$  GeV/c in 20-60% Zr+Zr collisions at  $\sqrt{s_{NN}} = 200$  GeV. Right: efficiency and acceptance corrected  $K^{*+}$  yield as a function of  $|\cos \theta^*|$  in 200 GeV Zr+Zr collisions.

37 At present, the available physics mechanisms that can cause spin align-  
 38 ment are the followings: (i) the polarized quarks induced by vorticity can  
 39 hadronize via coalescence mechanism. It can make  $\rho_{00}$  smaller than  $\frac{1}{3}$  [2, 6];  
 40 (ii) the  $\rho_{00}$  induced by the  $B$ -field can be either larger or smaller than  $\frac{1}{3}$ .  
 41 The expected deviation due to vorticity and  $B$ -field is  $\rho_{00} - \frac{1}{3} \sim 10^{-5}$  [6];  
 42 (iii) the electric field can give a positive contribution with  $\rho_{00} - \frac{1}{3} \sim 10^{-4}$  [6];  
 43 (iv) the fragmentation of polarized quarks can make either positive or neg-  
 44 ative contribution with  $\rho_{00} - \frac{1}{3} \sim 10^{-5}$  [2]; (v) local spin alignment, helicity  
 45 polarization, and turbulent color field can also make  $\rho_{00}$  smaller than  $\frac{1}{3}$  [7];  
 46 (vi) A fluctuating strong force field of vector meson can cause the  $\rho_{00}$  to  
 47 be larger than  $\frac{1}{3}$  with a deviation  $\sim 0.1$ , which is an order of magnitude

48 large compared to more conventional mechanisms [8]. The study of  $\rho_{00}$  of  
 49 various vector meson species can thus elucidate our understanding of dif-  
 50 ferent mechanisms causing spin alignment. Furthermore, the neutral and  
 51 charged vector mesons ( $K^{*0}(d\bar{s})$  and  $K^{*+}(u\bar{s})$ ) have similar mass, but the  
 52 magnetic moments of their constituent quarks differ by about a factor of  
 53 five ( $\mu_d \sim -0.97\mu_N$ ,  $\mu_u \sim 1.85\mu_N$ ). Hence, the magnetic field driven contri-  
 54 bution to the  $\rho_{00}$  of neutral and charged  $K^*$  is expected to be different.

55 The recent measurements of  $\rho_{00}$  of  $\phi$  and  $K^{*0}$  vector mesons from the  
 56 1<sup>st</sup> phase of RHIC Beam Energy Scan (BES-I) Au+Au collisions revealed a  
 57 surprising pattern [13]. While the  $K^{*0}$   $\rho_{00}$  is largely consistent with  $\frac{1}{3}$ , the  $\phi$   
 58 mesons show a large positive deviation ( $\rho_{00} > \frac{1}{3}$ ) with  $8.4\sigma$  significance when  
 59  $\rho_{00}$  is integrated within the range  $\sqrt{s_{NN}} = 11.5-62.4$  GeV for  $1.2 < p_T < 5.4$   
 60 GeV/ $c$  in 20-60% Au+Au collisions. Such a large positive deviation at mid-  
 61 central collisions pose challenges to more conventional physics mechanisms,  
 62 while the polarization induced from a fluctuating  $\phi$ -meson vector field can  
 63 accommodate the large positive signal [8]. Moreover, the  $p_T$  and centrality  
 64 differential measurements of  $\phi$  and  $K^{*0}$   $\rho_{00}$  in BES-I energy range also show  
 65 non-trivial patterns [13].

## 66 2. Analysis method

67 This proceedings report the first  $\rho_{00}$  measurements of charged  $K^{*\pm}$   
 68 along with neutral  $K^{*0}$  ( $\bar{K}^{*0}$ ) vector mesons in RHIC isobar collisions of  
 69  $^{96}_{44}\text{Ru}+^{96}_{44}\text{Ru}$  and  $^{96}_{40}\text{Zr}+^{96}_{40}\text{Zr}$  species at  $\sqrt{s_{NN}} = 200$  GeV [9]. The  $K^{*0}(\bar{K}^{*0})$   
 70 and  $K^{*+}(K^{*-})$  are reconstructed via  $K^{*0}(\bar{K}^{*0}) \rightarrow \pi^- + K^+(\pi^+ + K^-)$  and  
 71  $K^{*+}(K^{*-}) \rightarrow \pi^+ + K_S^0(\pi^- + K_S^0)$  respectively. The minimum-bias (MB)  
 72 events are collected via a coincidence between the Vertex Position Detec-  
 73 tors (VPD) located at  $4.4 < |\eta| < 4.9$ . For analysis, the vertex position  
 74 along the beam ( $V_{z,\text{TPC}}$ ) and radial direction ( $V_r$ ) are required to be within  
 75  $-35 < V_{z,\text{TPC}} < 25$  cm and  $V_r < 5$  cm respectively with a coordinate system  
 76 at the center of Time Projection Chamber (TPC). We analyzed about 1.8  
 77 and 2.0 billion good MB events for Ru+Ru and Zr+Zr collisions, respec-  
 78 tively. The charged particle tracking is performed using the TPC. The col-  
 79 lision centrality is determined from the number of charged particles within  
 80  $|\eta| < 0.5$ , and using a Monte Carlo Glauber simulation [10]. The second or-  
 81 der event plane ( $\Psi_{2,\text{TPC}}$ ) is reconstructed using the tracks inside TPC [11].  
 82 In isobar collisions, the typical  $\Psi_{2,\text{TPC}}$  resolution achieved in mid-central  
 83 collisions is  $R_{2,\text{TPC}} \sim 64\%$ . The decay daughters of  $K^*$  are identified us-  
 84 ing the specific ionization energy loss in TPC gas volume and the velocity  
 85 of particles measured by the TOF detector. The  $K_S^0$  mesons are selected  
 86 via a weak decay topology. For charged  $K^{*\pm}$  reconstruction, only the  $K_S^0$   
 87 candidates within  $0.48 < M(\pi^+\pi^-) < 0.51$  GeV/ $c^2$  are considered. The

88 combinatorial background is estimated from a track rotation technique, in  
 89 which one of the daughter track is rotated by  $180^\circ$  to break the correlation  
 90 among the pairs originating from same parent particle. Then, the invari-  
 91 ant mass signal is obtained by subtracting the combinatorial background.  
 92 The  $K^*$  signal is fitted with a Breit-Wigner distribution and a second-order  
 93 polynomial function to take care of residual background.

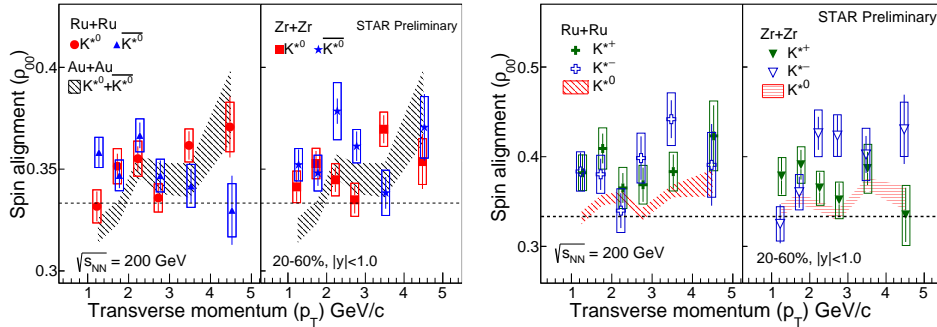


Fig. 2. Left:  $\rho_{00}(p_T)$  for  $K^{*0}$  and  $\overline{K}^{*0}$  in isobar collisions at  $\sqrt{s_{NN}} = 200$  GeV. Results are compared with that from 200 GeV Au+Au collisions [13]. Right: Comparison of  $\rho_{00}(p_T)$  between  $K^{*\pm}$  and  $K^{*0}$  in 200 GeV isobar collisions.

94 The left panel in Fig. 1 presents the  $K^{*+}$  signal for  $2.0 < p_T < 2.5$  GeV/ $c$   
 95 in 20-60% Zr+Zr collisions at  $\sqrt{s_{NN}} = 200$  GeV. The yield is estimated by  
 96 integrating residual background subtracted signal within the range:  $m_0 \pm 3\Gamma$ ,  
 97 where  $m_0$  and  $\Gamma$  are the invariant mass peak position and width of  $K^*$ . The  
 98 yield is obtained in five  $|\cos \theta^*|$  bins where  $\theta^*$  is the angle between  $\Psi_{2,TPC}$   
 99 and momentum of daughter kaon (pion) in parent  $K^{*0}$  ( $K^{*\pm}$ ) rest frame.  
 100 The detector acceptance and efficiency correction factors are obtained using  
 101 a STAR detector simulation in GEANT3. The right panel in Fig. 1 presents  
 102 efficiency and acceptance corrected  $K^{*+}$  yield as a function of  $|\cos \theta^*|$  for  
 103  $2.0 < p_T < 2.5$  GeV/ $c$  in 20-60% Zr+Zr collisions. The yield versus  $|\cos \theta^*|$   
 104 distribution is then fitted with Eq.1 and the extracted  $\rho_{00}$  (called  $\rho_{00}^{obs}$ ) is  
 105 corrected for event plane resolution using:  $\rho_{00} = \frac{1}{3} + \frac{4}{1+3R_{2,TPC}}(\rho_{00}^{obs} - \frac{1}{3})$  [12].

106

### 3. Results

107 The left panel of Fig. 2 presents the  $p_T$  dependence of  $\rho_{00}$  for  $K^{*0}$  and  
 108  $\overline{K}^{*0}$  at mid-rapidity ( $|y| < 1.0$ ) in 20-60% central Ru+Ru and Zr+Zr colli-  
 109 sions at  $\sqrt{s_{NN}} = 200$  GeV. The  $\rho_{00}$  between the particle and anti-particle  
 110 species are consistent within errors. These results are compared with that  
 111 from 200 GeV Au+Au collisions [13]. The  $\rho_{00}$  between isobar and Au+Au  
 112 collisions are consistent within uncertainties across the measured  $p_T$  region

113 in mid-central collisions. The right panel of Fig. 2 shows a comparison of  
 114  $\rho_{00}(p_T)$  among neutral and charged  $K^*$  species in isobar collisions. The  
 115  $\rho_{00}$  for charged  $K^{*\pm}$  are systematically larger than the neutral  $K^{*0}$  across  
 116 the measured  $p_T$  region. The left panel of Fig. 3 presents the  $\rho_{00}$  as a  
 117 function of average number of participants ( $\langle N_{\text{part}} \rangle$ ) for  $K^{*0}$  and  $\overline{K}^{*0}$  for  
 118  $1.0 < p_T < 5.0$  GeV/c in 200 GeV Ru+Ru and Zr+Zr collisions. These  
 119 results are compared with that from 200 GeV Au+Au collisions [13]. The  
 120  $K^{*0}$   $\rho_{00}$  is larger than  $\frac{1}{3}$  at smaller  $\langle N_{\text{part}} \rangle$ . It is smaller than  $\frac{1}{3}$  at large  
 121  $\langle N_{\text{part}} \rangle$ , which can have contributions from the local spin alignment [7]. At  
 122 a similar  $\langle N_{\text{part}} \rangle$ , the  $\rho_{00}$  between small system isobar and large system  
 123 Au+Au are comparable within uncertainties.

124 The right panel of Fig. 3 summarizes the  $p_T$ -integrated  $\rho_{00}$  for  $K^{*0}$ ,  $\overline{K}^{*0}$ ,  
 125  $K^{*+}$  and  $K^{*-}$  in 20-60% isobar collisions. These results are compared with  
 126  $(K^{*0} + \overline{K}^{*0})$   $\rho_{00}$  from Au+Au collisions [13]. This is the first observation  
 127 of  $K^{*\pm}$   $\rho_{00}$  to be larger than  $\frac{1}{3}$  in heavy-ion collisions. Moreover, the  $p_T$ -  
 128 integrated  $\rho_{00}$  reveals a clear ordering between neutral and charged  $K^*$   
 129 species in isobar collisions, with the charged species is about  $3.9\sigma$  larger  
 130 than the neutral ones. Due to the interaction between the  $B$ -field and the  
 131 magnetic moment of the constituent quarks, one naively expects the  $K^{*0}$   
 132  $\rho_{00}$  to be larger than that of  $K^{*\pm}$  [6]. But the observed ordering between  
 133  $K^{*0}$  and  $K^{*\pm}$  is opposite to such naive expectation. Although the reason  
 134 behind a difference between  $K^{*0}$  and  $K^{*\pm}$   $\rho_{00}$  is not understood yet, but  
 135 these species might have different contribution from the vector meson strong  
 136 force field. More inputs from theory are required to better understand the  
 137 underlying physics mechanisms.

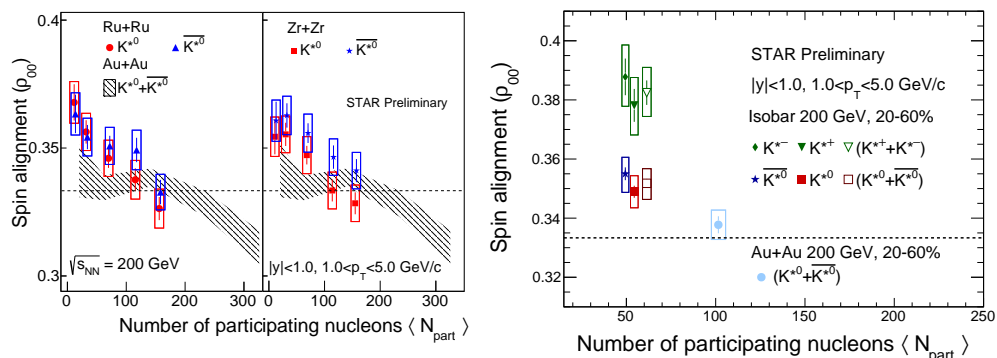


Fig. 3. Left:  $\rho_{00}(\langle N_{\text{part}} \rangle)$  for  $K^{*0}$  and  $\overline{K}^{*0}$  in isobar collisions at  $\sqrt{s_{\text{NN}}} = 200$  GeV. Right:  $p_T$  integrated  $\rho_{00}$  for  $K^{*0}$ ,  $\overline{K}^{*0}$ ,  $K^{*+}$  and  $K^{*-}$  in 20-60% 200 GeV isobar collisions. Results are compared with  $K^{*0}$  in 200 GeV Au+Au collisions [13].

138

#### 4. Summary and conclusion

139 In summary, the measurements of  $\phi$  and  $K^{*0}$   $\rho_{00}$  in Au+Au collisions  
 140 from RHIC BES-I reveal a surprising pattern with a large positive deviation  
 141 from  $\frac{1}{3}$  for  $\phi$  mesons and no obvious deviation for  $K^{*0}$ . At present, a fluctuating  
 142 vector meson strong force field can accommodate the large positive  
 143 deviation for  $\phi$  mesons, while more theory inputs are needed for  $K^{*0}$ . The  
 144 recent high statistics RHIC isobar collision (Ru+Ru and Zr+Zr) data offer  
 145 a new opportunity to extend the measurement of  $\rho_{00}$  for  $K^{*0}$ ,  $\overline{K}^{*0}$ ,  $K^{*+}$ ,  
 146 and  $K^{*-}$  vector mesons with high precision. We observe the first non-zero  
 147 spin alignment for  $K^{*\pm}$  in heavy-ion collisions. The  $K^{*\pm}$   $\rho_{00}$  is larger than  
 148 that of  $K^{*0}$  for 20-60% central isobar collisions. The current large deviation  
 149 of  $K^{*\pm}$   $\rho_{00}$  and its ordering with  $K^{*0}$  is surprising, and opposite to the  
 150 naive expectation from  $B$ -field. These results pose challenges to current un-  
 151 derstanding and inputs from theory are required to interpret the  $\rho_{00}$  results  
 152 from isobar data.

#### REFERENCES

- 153 [1] F. Becattini, *et al.*, Phys. Rev. **C77** (2008) 024906  
 154 [2] Z. T. Liang and X. N. Wang, Phys. Lett. **B629** (2005) 2026  
 155 [3] D. Kharzeev *et al.*, Nucl. Phys. **A803** (2008) 227-253  
 156 [4] L. Adamczyk *et al.*, [STAR Collaboration], Nature **548** (2017) 6265; J. Adam  
 157 *et al.*, [STAR Collaboration], Phys. Rev. **C98** (2018) 014910  
 158 [5] K. Schilling *et al.*, Nucl. Phys. **B15** (1970) 397412  
 159 [6] Y. G. Yang *et al.*, Phys. Rev. **C97** (2018) 034917  
 160 [7] X. L. Xia *et al.*, Phys. Lett. **B817** (2021) 136325; J. H. Gao, Phys. Rev.  
 161 **D104** (2021) 076016 076016; B. Müller and D. Yang Phys. Rev. **D105** (2022)  
 162 L011901  
 163 [8] X. Sheng *et al.*, Phys. Rev. **D101** (2020) 096005; Phys. Rev. **D102** (2020)  
 164 056013; arXiv 2206.05868;  
 165 [9] M. Abdallah *et al.*, [STAR Collaboration], Phys. Rev. **C105** (2022) 014901  
 166 [10] B. I. Abelev *et al.*, [STAR Collaboration], Phys. Rev. **C79** (2009) 034909  
 167 [11] A. M. Poskanzer and S. A. Voloshin, Phys. Rev. **C58** (1998) 16711678  
 168 [12] A. H. Tang *et al.*, Phys. Rev. **C98** (2018) 044907  
 169 [13] M. Abdallah *et al.*, [STAR Collaboration], arXiv:1910.14408